

# Fully implicit moving boundary model with liquid phase perfect mixing for CO<sub>2</sub> diffusion into n-decane

DAMELYS ZABALA<sup>1</sup>, AURA L. LÓPEZ DE RAMOS<sup>2</sup>

<sup>1</sup>CIMEC, Escuela de Ingeniería Mecánica, <sup>2</sup>Departamento de Termodinámica y Fenómenos de Transferencia

<sup>1</sup>Universidad de Carabobo, <sup>2</sup>Universidad Simón Bolívar

<sup>1</sup>Av. Universidad, Edf. Facultad de Ingeniería, Bárbula, Estado Carabobo, <sup>2</sup>Apartado Postal 89.000, Caracas VENEZUELA

<sup>1</sup>dzabala@uc.edu.ve, <sup>2</sup>alopez@usb.ve

**Abstract:** - Carbon dioxide diffusion into n-decane inside cylindrical and square glass capillary tubes has been modeled [1,2], with two different models for each tube and the convective model for the square tube depended on the results of the cylindrical one. For those models, the liquid phase density was always considered constant and its value was adjusted from the experimental data of gas-liquid interface position. This approach was done using the diffusivities obtained by correlations which modify the infinite dilution diffusion coefficient using a thermodynamical factor. Now, the liquid phase density is considered variable on time with perfect mixing inside the phase and an effective diffusivity can be determined. This effective diffusivity involves the molecular and convective contributions to the global mass transfer. Both interface displacements (inside cylindrical and square tubes) can be modeled using the same model without dependency between their results. The terms inside the finite difference matrix for the liquid phase are not constant, because they depend on the solute concentration and on the liquid density then an iterative calculation for the matrix coefficients must be done in each timestep. A partially implicit model considers this iterative calculation keeping the liquid density value for the previous time (j). A fully implicit model considers this iterative calculation keeping the liquid density value for the present time (j+1). It was showed that the model results, adjusted to the experimental interface position values, predicted effective diffusivities which are variable on time. The simulation time (76 min) for the fully implicit numerical model is higher than the simulation time (62 min) for the partially implicit numerical model. It was found that the type of numerical solution scheme affects the results (up to 5% deviation) for the square capillary model but it doesn't change the cylindrical capillary model results.

**Key-Words:** - Capillary tube, Free boundary, Mass transfer, Numerical Modeling, Diffusion

## 1 Introduction

Numerical modeling is an useful tool for representing heat and mass transfer processes. In many cases, numerical solution of a differential equation is used together with an experiment in order to determine fluid properties. For example, to obtain mass diffusivities by experimental methods usually involves mathematical simplification, like constant phase density and no convective effects [3-5]. Estimation of mass diffusivities is always a major concern for mass transfer processes, because correlations are not applicable in all the systems or process conditions. On the other hand, fluid displacement inside polygonal capillary tubes or cells has been studied trying to understand fluid-solid interactions in porous media [6-13]. The corners of capillary tubes promote fluid movement by a liquid filament which rises along the crevice and this behavior avoided that displacement experiments in polygonal capillary tubes could be used to determine molecular diffusivity because a simplified mass

transfer model deviates considerably from the experimental behavior. In this work, experiments with carbon dioxide diffusing into liquid n-decane were done, with both fluids contained in square and cylindrical glass capillary tubes. Experimental gas-liquid interface positions at the center of the tube were observed and it was found that the interface moves faster inside the square capillary tube. A moving boundary mass transfer model of this miscible displacement is necessary, to determine the contribution of the corner presence to an improved mass transfer process like the miscible CO<sub>2</sub> injection in hydrocarbons. Such contribution is determined by adjustment of an effective diffusivity which counts for molecular and convective mass transfer.

## 2 Problem Formulation

### 2.1 Mathematical Model

For a component “i”, the one-dimension continuity equations for liquid and gas phases are: [14-16]

$$\frac{\partial \rho_{i,L}}{\partial t} + \frac{\partial n_{i,L}}{\partial z} = 0, \quad 0 \leq z \leq s(t) \quad (1)$$

$$\frac{\partial \rho_{i,G}}{\partial t} + \frac{\partial n_{i,G}}{\partial z} = 0, \quad s(t) \leq z \leq L \quad (2)$$

For the liquid phase, the global mass balance is shown in eq.(3) and the total flux  $n$  can be related to the diffusive flux  $j$ . [15]

$$\frac{d(\rho_L V)}{dt} = -\rho_L U_s A_r \quad (3)$$

$$j_i + \rho U^{ref} = n_i \quad (4)$$

The reference velocity for the phase ( $U^{ref}$ ) can be defined in different ways. One of them, is the average mass velocity, and for a binary mixture “i,j” can be expressed by:

$$U^{mass} = \frac{\sum \rho_j U_j}{\rho} = \frac{n_i + n_j}{\rho} = \frac{n}{\rho} \quad (5)$$

Equation (5) is replaced in equation(4), and defining an effective diffusivity, the total flux can be related to concentration gradient by the Fick law, eq.(7). The thermodynamical factor  $Q$  depends on the solute concentration.

$$n_i = j_i + w_i n \quad (6)$$

$$n_i = -D_L \frac{\partial \rho_i}{\partial z} = -(D_{ef} Q) \frac{\partial \rho_i}{\partial z} \quad (7)$$

For carbon dioxide, one-dimension continuity equations for liquid and gas phases are: [14-16]

$$\frac{\partial \rho_C}{\partial t} = \frac{\partial}{\partial z} \left( D_L \frac{\partial \rho_C}{\partial z} \right), \quad 0 \leq z \leq s(t) \quad (8)$$

$$\frac{\partial y_C}{\partial t} = D_G \frac{\partial^2 y_C}{\partial z^2}, \quad s(t) \leq z \leq L \quad (9)$$

Equations (8) and (9) are for mass transfer process without chemical reaction. Equation (8) includes convective effects through the effective diffusivity  $D_{ef}$  and the liquid phase is calculated, using equation (3). The CO<sub>2</sub> mass concentration  $\rho_C$ , can be related to mass fraction  $w_C$  using equation (10).

$$\rho_C = w_C \rho_L \quad (10)$$

The initial and boundary conditions are in Table 1. Making a mass balance for carbon dioxide across the moving interface, its position can be determined by solving the ordinary differential equation (11). [14,17, 18]

$$\rho_L D_L \frac{\partial w_C}{\partial z} \Big|_{z=s(t)^-} - \rho_G D_G \frac{\partial y_C}{\partial z} \Big|_{z=s(t)^+} = \left( y_C^{sat} \rho_G - w_C^{sat} \rho_L \right) \frac{ds(t)}{dt}, \quad z = s(t) \quad (11)$$

Following the methodology developed by Illingworth and Golosnoy[14], the moving boundaries are transformed in fixed ones, by definition of new spatial variables  $u$  and  $v$ . The mass fractions are defined by new dependant variables  $p$  and  $q$ .

$$u = \frac{z}{s(t)}, \quad v = \frac{z-s(t)}{L-s(t)}$$

$$p(u,t) = w_C(z,t), \quad q(v,t) = y_C(z,t)$$

Table 1. Initial and border conditions

Gas phase	Liquid phase
$t = 0, \quad y_C = y_C^{ini}$	$t = 0, \quad \rho_L = \rho_L^{ini}$
	$t = 0, \quad w_C = w_C^{ini}$
$z = s(t), \quad y_C = y_C^{sat}$	$z = s(t), \quad w_C = w_C^{sat}$
$z = L, \quad y_C = y_C^{ini}$	$z = 0, \quad \frac{\partial w_C}{\partial z} = 0$

The transformed equations inside the phases are (12) and (13), and their respective transformed initial and boundary conditions are in Table 2.

$$\frac{\partial (p \rho_L)}{\partial t} - U_s \frac{u \rho_L}{s} \frac{\partial p}{\partial u} = \rho_L \frac{\partial}{\partial u} \left( \frac{D_L}{s^2} \frac{\partial p}{\partial u} \right), \quad 0 \leq u \leq 1 \quad (12)$$

$$\frac{\partial q}{\partial t} - U_s \frac{1-v}{L-s} \frac{\partial q}{\partial v} = \frac{\partial}{\partial v} \left( \frac{D_G}{(L-s)^2} \frac{\partial q}{\partial v} \right), \quad 0 \leq v \leq 1 \quad (13)$$

Table 2. Transformed initial and border conditions

Gas phase	Liquid phase
$t = 0, \quad q = y_C^{ini}$	$t = 0, \quad p = w_C^{ini}$
$v = 0, \quad q = y_C^{sat}$	$u = 1, \quad p = w_C^{sat}$
$v = 1, \quad q = y_C^{ini}$	$u = 0, \quad \frac{\partial p}{\partial u} = 0$

The transformed interface equation (14) is converted to an expression, eq.(15), which conserves solute [14].

$$\rho_L \frac{D_L}{s} \frac{\partial p}{\partial u} \Big|_{u=1} - \rho_G \frac{D_G}{L-s} \frac{\partial q}{\partial v} \Big|_{v=0} = \left( y_C^{sat} \rho_G - w_C^{sat} \rho_L \right) \frac{ds(t)}{dt}, \quad u = 1, \quad v = 0 \tag{14}$$

$$\frac{\partial}{\partial t} \left\{ s(t) \rho_L \int_0^1 p(u,t) du + (L-s(t)) \rho_G \int_0^1 q(v,t) dv \right\} = 0 \tag{15}$$

For discretisation, the liquid phase equation is written in a divergent form, eq.(16) , and it is integrated, eq. (17), between the indicated  $u$  and  $t$  intervals, defined according equation (18).

$$\frac{\partial (sp\rho_L)}{\partial t} = \frac{\partial}{\partial u} \left( U_s u p \rho_L + \frac{D_L}{s} \frac{\partial (p\rho_L)}{\partial u} \right) \tag{16}$$

After the first integration equation (17) is transformed in eq. (19). For the second integration, these are the considerations. For the left side of eq.(19),  $p$  is considered constant for the  $u$  integration interval.

$$\int_{u_{i-1/2}}^{u_{i+1/2}} \int_{t^j}^{t^{j+\sigma}} \frac{\partial (sp\rho_L)}{\partial t} dt du \tag{17}$$

$$= \int_{t^j}^{t^{j+\sigma}} \int_{u_{i-1/2}}^{u_{i+1/2}} \frac{\partial}{\partial u} \left( U_s u p \rho_L + \frac{\rho_L D_L}{s} \frac{\partial p}{\partial u} \right) du dt$$

$$u_{i+1/2} = \frac{u_i + u_{i+1}}{2}; \quad u_{i-1/2} = \frac{u_i + u_{i-1}}{2} \tag{18}$$

$$\int_{u_{i-1/2}}^{u_{i+1/2}} \left\{ p^{j+1} s^{j+1} \rho_L^{j+1} - p^j s^j \rho_L^j \right\} du = \int_{t^j}^{t^{j+1}} \left\{ \left( U_s p_{i+1/2} u_{i+1/2} \rho_L + \frac{\rho_L (D_L)_{i+1/2}}{s} \frac{\partial p}{\partial u} \Big|_{i+1/2} \right) - \left( U_s p_{i-1/2} u_{i-1/2} \rho_L + \frac{\rho_L (D_L)_{i-1/2}}{s} \frac{\partial p}{\partial u} \Big|_{i-1/2} \right) \right\} dt \tag{19}$$

For the right side of eq.(19),  $p$  and other time functions are considered constant for the  $t$  integration

interval defining the parameter  $\sigma$  ( $0 \leq \sigma \leq 1$ ). This constant value is defined according eq. (20).

$$p_i^{j+\sigma} = \sigma p_i^{j+1} + (1-\sigma) p_i^j \tag{20}$$

Equation (21) is the general finite difference scheme for the mass fraction in the liquid phase, except for the border points. This scheme will be fully implicit when  $\sigma=1$ . It will be partially implicit when  $\sigma=1$  for all the terms except for  $\rho_L$ , where  $\sigma=0$ . For the liquid phase density, equation (3) is discretised and the finite difference scheme is shown in eq. (24). For the gas phase, the general finite difference scheme is the same developed by Illingworth and Golosnoy [14].

$$\frac{p_i^{j+1} \left[ \left( r_{i+1/2}^{j+1} \right) - \left( r_{i-1/2}^{j+1} \right) \right] - p_i^j \left[ \left( r_{i+1/2}^j \right) - \left( r_{i-1/2}^j \right) \right]}{(t^{j+1} - t^j)} = \left\{ \left[ U_s^{j+\sigma} p_{i+1/2}^{j+\sigma} u_{i+1/2} \rho_L^{j+\sigma} + \frac{\rho_L^{j+\sigma} (D_L)_{i+1/2}}{s^{j+\sigma}} \frac{\partial p}{\partial u} \Big|_{i+1/2}^{j+\sigma} \right] - \left[ U_s^{j+\sigma} p_{i-1/2}^{j+\sigma} u_{i-1/2} \rho_L^{j+\sigma} + \frac{\rho_L^{j+\sigma} (D_L)_{i-1/2}}{s^{j+\sigma}} \frac{\partial p}{\partial u} \Big|_{i-1/2}^{j+\sigma} \right] \right\} \tag{21}$$

$$r_{i\pm 1/2}^j = \rho^j s^j u_{i\pm 1/2} \tag{22}$$

$$\rho_L^{j+1} A_T s^{j+1} - \rho_L^j A_T s^j = -\rho_L^{j+1} U_s A_T \Delta t \tag{23}$$

$$\rho_L^{j+1} = \frac{\rho_L^j s^j}{2s^{j+1} - s^j} \tag{24}$$

This mathematical model in one dimension does not consider the real shape of the interface, with a meniscus (both tubes) and the filaments in the corners of the square tube.(Fig.1).

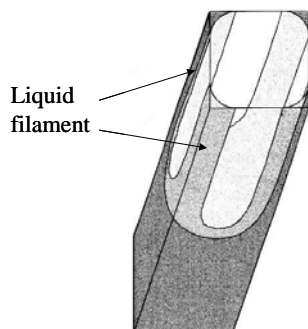


Fig. 1. Meniscus and filament (square capillary tube)

## 2.2 Experimental Equipment

A visualization cell was built with two plexiglass caps (2 cm thickness) and four common glass walls (5 cm thickness), the joints are sealed with silicon. A scale for interface displacement measurement is marked on the capillary tube surface, before the tube is put inside the cell. The space between marks is 5 mm. The capillary tube is fixed to brass connectors in upper and lower extremes of the cell using epoxy glue (Fig. 2). The space between the capillary and the cell walls is filled with glycerol (99.5%) which has the same refractive index than the glass, to avoid distortion by light diffraction. The cell is joined to a metallic base by, at least, two long screws passed through to aligned holes in both plexiglass caps. The screws are supported to the caps by washers and nuts. The distance from the lowest mark and the lower extreme of the tube is recorded as well as the capillary tube length. The cell assembly is on a pneumatic vibration isolated table to minimize movement in the system. In the capillary lower extreme, a membrane is put between the tube and the brass connector to seal this side during the test. Before the test, system leaks are checked, flowing carbon dioxide at the test pressure for at least five minutes. If there are no leaks, system returns to atmospheric pressure and then the hydrocarbon (n-C10: n-Decane) is injected by the lower extreme, passing a syringe through a small hole in the connector and penetrating the membrane. The carbon dioxide is injected through the upper side at 23.5 °C and 1480 kPa (abs) and the recording process begins. The camcorder is a Sony mini DV, model DCR-HC42 with a 12X macro lens, positioned in a way that the meniscus can be observed between the marks on the capillary (Fig. 3). The space between marks is 5 mm, so it is possible to have the calibration pixel/mm direct from the test images. Capillary tube data are shown in table 3.



Fig.2. Joint capillary tube/brass conector

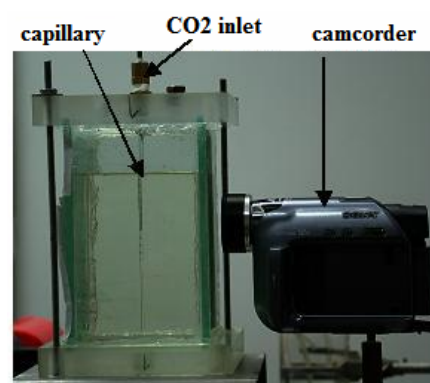


Fig.3. Visualization cell

Table 3. Capillary tube data

Capillary	Cylindrical	Square
L[mm]	194	210
ID [mm]	Diameter	Side
	2	2
Material	Borosilicate	Quartz

## 3 Problem Solution

### 3.1 Mathematical Model Results

Diffusion coefficients are considered variable in liquid phase and constant in gas phase. For  $D_L$  estimation, eq.(25), the thermodynamic factor  $Q$ , eq. (26), is calculated using activity coefficient estimated by Margules with two subscripts and the  $A$  parameter for this model was determined for a previous model [2].

$$D_L = D_{ef} Q \quad (25)$$

$$Q = 1 - p \frac{2A}{RT} (1 - p) \quad (26)$$

$D_G$  is calculated by Wilke and Lee correlation [19].  $C_G$  is approximated to pure  $CO_2$  molar density which it is calculated by Pitzer and Sterner equation of state [20]. Calculated and experimental data are shown in Table 4.

The partial derivative equation system (12), (13) and (15) is discretised and numerically solved by finite difference method. The algorithms used are of first order accuracy [14]. The space discretisation is done with a fixed mesh for gas phase and with three different step sizes for liquid phase, the smallest one near the interface (Table 5). The time discretisation is done with four different time step sizes, because very small time step improves the solution stability but increases the simulation time as it was found when the no convective model was solved [22]. Two finite difference solution schemes are used: partially implicit and fully implicit. The algorithms for each case are explained in the next paragraphs.

Table 4. Data at P=1480 kPa, T=23.5 °C

$y_C^{sat}$	0.998 [21]	$D_G$ [m <sup>2</sup> /s]	$5.9 \cdot 10^{-7}$
$y_C^{ini}$	1	A [kJ/kmol]	7900 [2]
$w_C^{sat}$	0.067 [21]	$\rho_G$ [kg/m <sup>3</sup> ]	28.7
$w_C^{ini}$	0	$\rho_L^{ini}$ (nC10 pure) [kg/m <sup>3</sup> ]	680.92

Table 5 .Time and space step sizes

Variable range	Step size
$0 \leq v \leq 1$	$\Delta v = 0.05$
$0 \leq u \leq 0.7$	$\Delta u = 0.14$
$0.7 < u \leq 0.9$	$\Delta u = 0.05$
$0.9 < u \leq 1$	$\Delta u = 0.1/135$
$t < 2$ s	$\Delta t = 10^{-2}$ s
$2 \leq t < 60$ s	$\Delta t = 2 \cdot 10^{-2}$ s
$60 \leq t \leq 90$ s	$\Delta t = 5 \cdot 10^{-2}$ s
$t > 90$ s	$\Delta t = 10^{-1}$ s

➤ **Partially-implicit model**

The algorithm for this case is shown in Fig.4. The finite difference solution scheme is partially implicit, because the concentration terms present in the liquid phase for  $D_L$  are evaluated in the present time ( $\sigma=1$ ). Then, the finite difference matrix has variable coefficients and for that reason an iterative calculation process must be done for each time step in order to obtain the solution for the liquid concentration profile. However, the liquid density is

evaluated in the previous time ( $\sigma = 0$ ) and for this reason the algorithm is considered partially implicit.

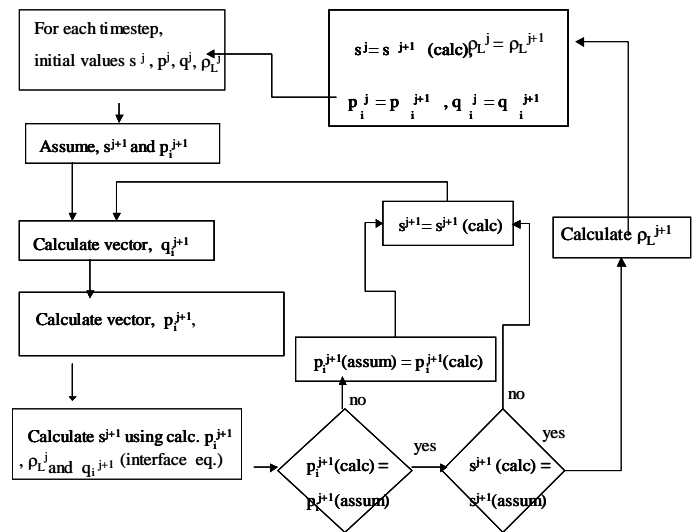


Fig.4. Algorithm- partially implicit model

➤ **Fully implicit model**

The algorithm for this case is shown in Fig.5.

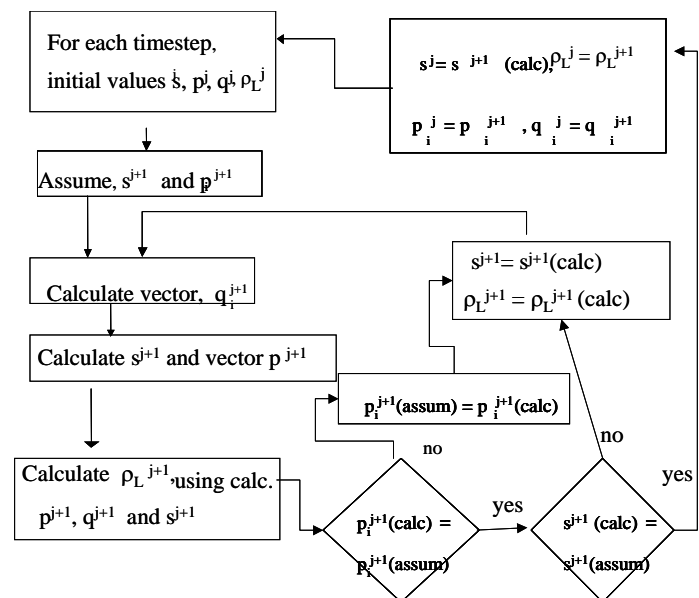


Fig.5. Algorithm- fully implicit model

The finite difference solution scheme is fully implicit, because the concentration terms present in the liquid phase for  $D_L$  are evaluated in the present time ( $\sigma=1$ ). In this case, also, the finite difference

matrix has variable coefficients and the iterative calculation also must be done in this case. Additionally in this case, the liquid density is also evaluated in the present time ( $\sigma=1$ ) and it is recalculated inside the iterative process together with the interface position and concentration profiles. For this reason the algorithm is considered fully implicit. This additional iterative calculation is shown in Fig. 5.

### 3.2 Experimental Results

Images of cylindrical and square capillary experimental interface positions are shown in figures 6 and 7.

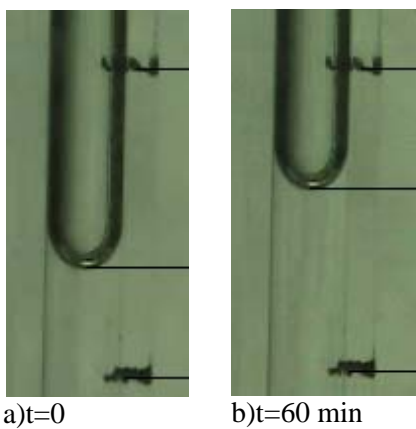


Fig.6. Displacement inside cylindrical capillary

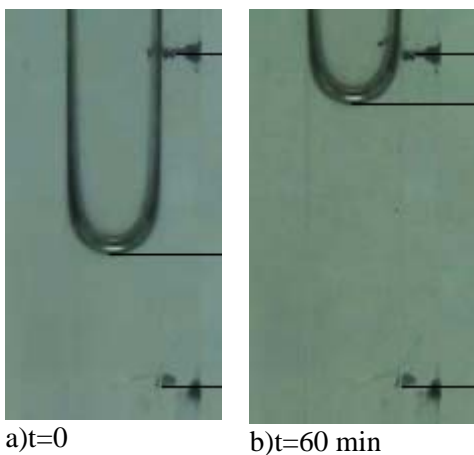


Fig.7. Displacement inside square capillary

The experimental results for interface displacement,  $s(t)$ , relative to its initial position,  $s(0)$ , are compared with the results predicted by the partially implicit numerical model as it is shown in Fig.8. Experimental interface displacement for the square capillaries is larger than the displacement for cylindrical ones. This behavior is similar to the reported by other authors, in experiments done at

different temperature and pressure and with other saturated hydrocarbons [3,5,6].

Fig. 9 shows the partially implicit model results for the interface displacement inside cylindrical capillary tube. Fig. 10 shows the partially implicit model results for the interface displacement inside square capillary tube. Simulation time is 62 min in both cases, which is considerably higher than the simulation time for the previous models [1,2].

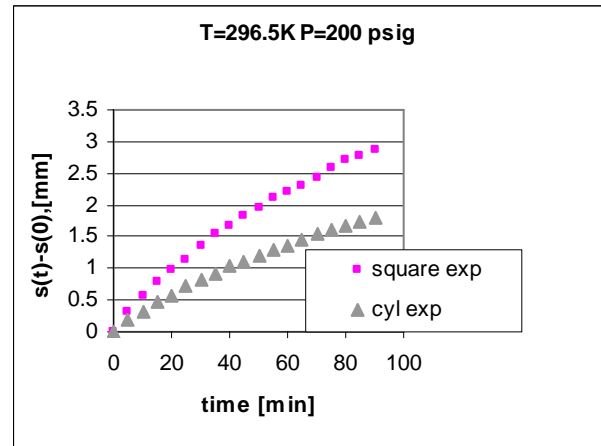


Fig.8. Experimental results comparison

For the cylindrical capillary tubes, a small deviation is observed from the experimental curve (fig. 9). The average relative error for the cylindrical model is 9.3%. For the square capillary tubes, there is no significant deviation from the experimental data (fig. 10). The average relative error for the square model is 3.1%. These deviations are similar to the deviations in previous simple models [1,2] but for the case of square capillary model, the deviation is considerably smaller than the one found in the models proposed by Garrido (60%) and De Freitas (32%) [5,6], where analytical solutions were used.

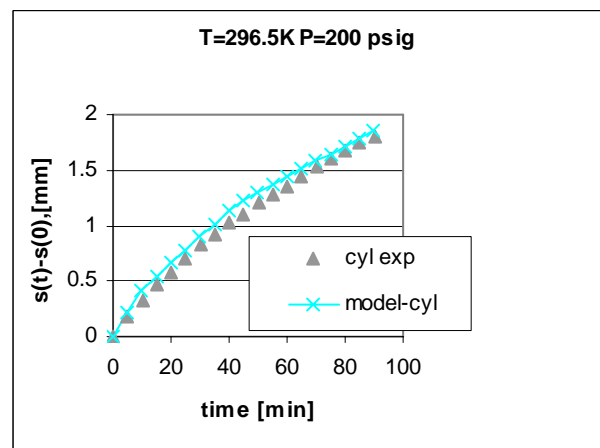


Fig.9. Interface displacement-Cylindrical

The other results for both capillary tube shapes can be observed in the figures 11 and 12. Those results are also for the partially implicit model.

In Fig. 11, a reduction in the liquid density is observed inside both capillary tubes, being more drastic for the square capillary. It can be explained by the presence of the liquid filaments in the corners of the square capillary tube, which improves the mixing in the liquid phase. A similar trend is observed in the reduction of the liquid effective diffusivity (Fig.12).

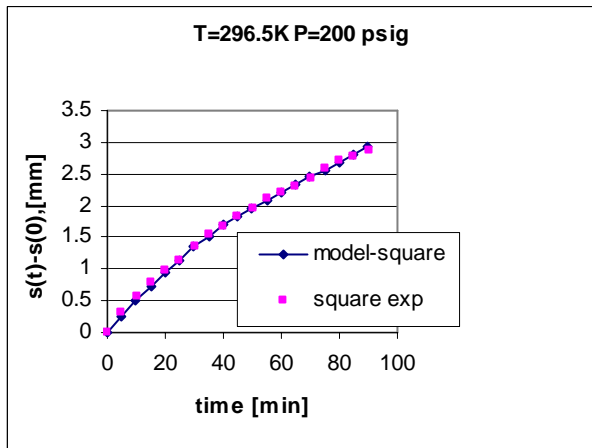


Fig.10. Interface displacement-square

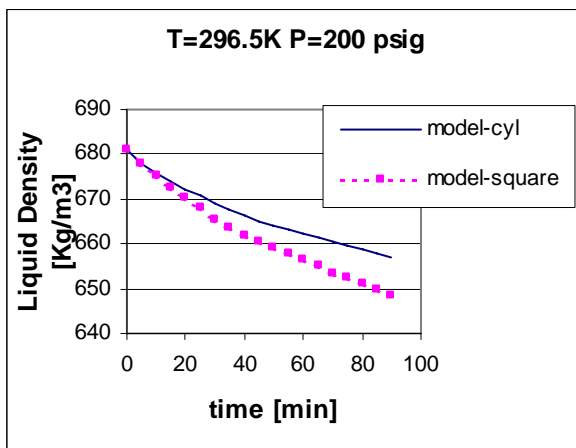


Fig.11. Liquid density - model result comparison

However, the effective diffusivity in the square capillary tube is considerably higher than the diffusivity for diluted solution, estimated by Scheibel correlation [23], used in previous models [1,2] for the diffusivity estimation. Only at the end of the experiment, both diffusivities are similar for the square capillary tube. This behavior can be explained because the driven force is reduced by the dissolved CO<sub>2</sub> into the hydrocarbon at this moment. The improved mixing induced by the liquid filaments, may be is also responsible for the higher effective

diffusivity in the square capillary tubes. In cylindrical capillary tubes, the average *Def* is similar to the diluted solution diffusivity, which can be explained because inside the cylindrical capillary tube, the convective contribution to the effective diffusivity is small in comparison with the molecular one, due to the absence of corners with the liquid filaments.

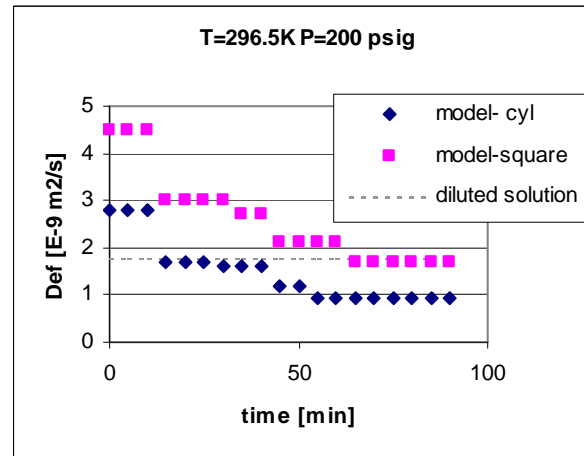


Fig.12. Effective diffusivity- model result comparison

➤ Fully implicit vs partially implicit model

The fully implicit model increases the simulation time up to 76 min in comparison with the partially implicit model (62 min). The additional time can be consequence of the modified algorithm, where the recalculation of the liquid phase density is done together with the interface position (Fig. 5).

In order to determine if the numerical solution scheme affects the model results and if the extra calculation time is necessary, a comparison between both solutions is done for the cylindrical and square capillary tubes. The results are shown in figures 13 to 16.

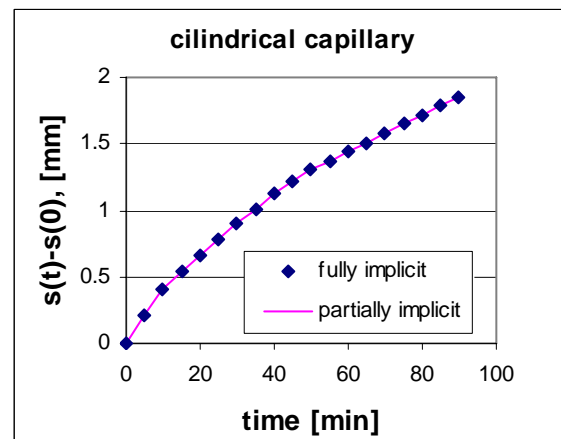


Fig.13. Displacement – different models (cylindrical)

The results for cylindrical capillary tube are shown in figures 13 and 14. Fig. 13 shows the interface displacement results. It is observed that there is no difference between the predicted results by both numerical solution schemes for the interface displacement inside cylindrical capillary tubes. Fig. 14 shows the liquid density results. It is observed the same behavior that for the interface displacement: there is no difference between the predicted results by both models.

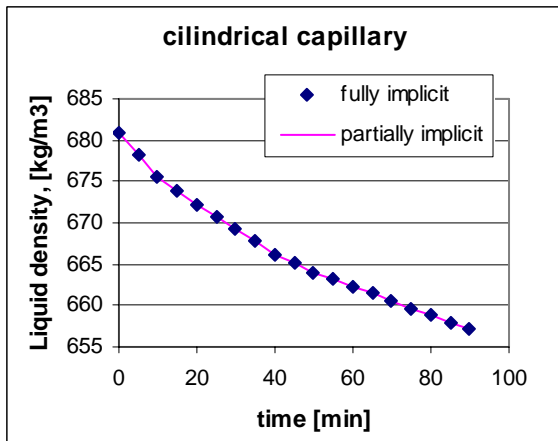


Fig.14.Liquid density– different models (cylindrical)

The results for square capillary tube are shown in figures 15 and 16. In this case, there is a difference between the predicted results for the liquid density and the interface displacement, depending on the numerical solution scheme. For the interface displacement (Fig. 15), the average deviation between both models is 5.3%. For the liquid density (Fig. 16), the average deviation between both models is 0.11%.

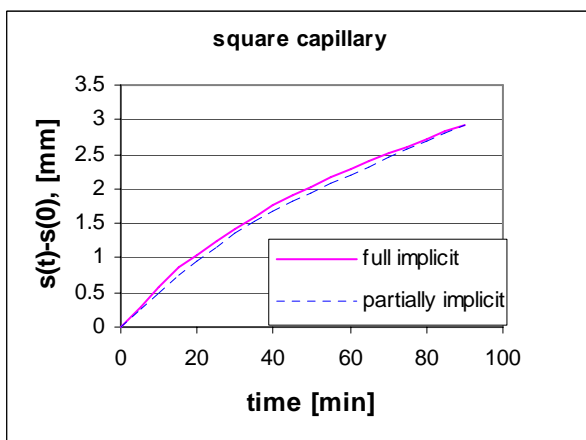


Fig.15. Displacement – different models (square)

These results suggest that the mass transfer process inside the cylindrical capillary tube is slower than

inside the square tube and because of that, the density and composition changes in the liquid phase are not affected for the type of numerical solution.

On the other hand, inside the square capillary tube, the mixing speed in the liquid phase can be increased by a convective effect induced by the liquid filaments, rising along the corners of the capillary tube. This improved mixing makes that the liquid density and composition changes in the liquid phase are more affected for the numerical solution scheme. As a consequence of this, the calculation of interface position is also affected.

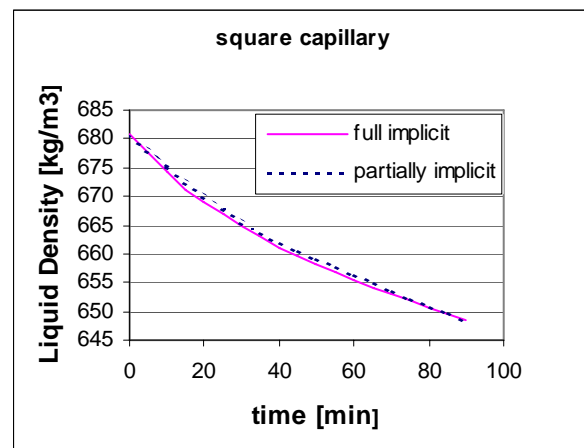


Fig.16. Liquid density– different models (square)

#### 4 Conclusion

This more complex mass transfer model, which considers both variable liquid diffusion coefficient and liquid density, is better to represent interface displacement in a CO<sub>2</sub> diffusion process in liquid n-C10, inside capillary tubes, having the advantage of that square capillary tube model is not dependent on the results of the cylindrical one. The capillary tube shape effects can be observed in the variation in the liquid effective diffusivity and in the liquid density. The disadvantage against previous simplified models [1,2] is the increase in the simulation time. The diffusion model for cylindrical capillary tubes can be numerical solved with a partially implicit solution scheme, because the results are not affected by this factor. For the diffusion model in square capillary tubes, is better to use the fully implicit model, because the results change according the chosen solution scheme. This behavior is explained because the improved mass transfer inside square capillary tube produces faster changes in density and composition which are affected by the type of the numerical solution.

*List of Symbols*

$A_T$ = mass transfer area, [m<sup>2</sup>]  
 Def= Effective CO<sub>2</sub> diffusion coefficient in liquid phase, [m<sup>2</sup>/s].  
 $j$ = Mass diffusive flux, [kg/(m<sup>2</sup> s)]  
 $L$ = capillary tube length, [m].  
 $n$ = Mass total flux, [kg/(m<sup>2</sup> s)]  
 $P$ = absolute pressure, [kPa]  
 $Q$ = thermodynamical factor [-]  
 $R$ = 8.3144 kJ/kmol K  
 $s=s(t)$ = interface position, relative to capillary tube bottom [m].  
 $U_S$ = interface velocity, [m/s].  
 $V$ = Liquid phase volume, [m<sup>3</sup>]  
 $T$ = temperature, [K]  
 $w_C$ = CO<sub>2</sub> mass fraction in liquid phase, [-].  
 $y_C$ = CO<sub>2</sub> mass fraction in gas phase, [-].

*Greek letters*

$\rho_k$ = mass density of "k" phase, [kg/m<sup>3</sup>].

<i>Subscripts</i>	<i>Superscripts</i>
L= liquid phase	ini= initial
G= gas phase	sat= saturation

*Acknowledgement*

The authors want to thank CDCH-Universidad de Carabobo (Project N° 2007-001) and Fonacit (S1-2001-000778) for their financial support.

*References:*

- [1] Zabala, D.; López de Ramos, A. Effect of the Finite Difference Solution Scheme in a Free Boundary Convective Mass Transfer Model. *WSEAS Transactions on Mathematics*, Vol.6, N° 6, 2007, pp.693-700.
- [2] Zabala, D.; López de Ramos, A. Solute concentration effect in gas-liquid interface displacement modeling. *WSEAS Transactions on Fluid Mechanics*, Vol.1, N° 6, 2006, pp. 686-691.
- [3] López de Ramos, A. *Capillary enhanced diffusion of CO<sub>2</sub> in porous media*. Ph.D. Dissertation, University of Tulsa, U.S.A, 1993.
- [4] Grogan, A.; Pinczewski, V.; Ruskauff, G.; Orr, F. Diffusion of carbon dioxide at reservoir conditions: Models and Measurements. Paper SPE/DOE 14897, presented at *SPE/DOE Fifth Symposium on Enhanced Oil Recovery*, Tulsa, OK, Apr. 20-23, 1986.
- [5] Garrido, A. *Estudio Teórico Experimental de la Transferencia de Masa en Líquidos Confinados en Regiones con Angularidades*. M.Sc Thesis, Universidad Simón Bolívar, Venezuela, 2005.
- [6] De Freitas, A. *Estudio del efecto de las esquinas en la transferencia de masa en medios porosos*. M.Sc Thesis, Universidad Simón Bolívar, Venezuela, 2005.
- [7] Lenormand, R.; Zarcone, C. Role of roughness and edges during imbibition in square capillaries. Paper SPE 13264, presented at the *59<sup>th</sup> Annual Technical Conference and Exhibition of the Society of Petroleum Engineers of AIME*, Houston, Texas, Sept. 16-19, 1984.
- [8] Patzek, T.W.; Kristensen, J.G. Shape Factor and Hydraulic Conductance in Noncircular Capillaries I: One-Phase Creeping Flow. *J. of Colloid and Interface Science*, Vol. 236, 2001, pp.295-304.
- [9] Patzek, T.W.; Kristensen, J.G. Shape Factor Correlations of Hydraulic Conductance in Noncircular Capillaries II: Two-Phase Creeping Flow. *J. of Colloid and Interface Science*, Vol. 236, 2001, pp.305-317.
- [10] Simmons, M.; Wong, D.; Travers, P.; Rothwell, J. Bubble Behaviour in Three Phase Capillary Microreactors. *International Journal of Chemical Reactor Engineering*, Vol 1, 2003, A30.
- [11] Patrick, R. Jr.; Klindera, T.; Crynes, L.L., Cerro, R.L. y Abraham, M.A. Residence time distribution in three-phase monolith reactor. *AIChE Journal*, Vol. 41, 2004, 649-657.
- [12] Firincioglu, T.; Blunt, M.; Zhou, D. Three-phase flow and wettability effects in triangular capillaries. *Colloids and Surfaces A*, Vol. 155, 1999, pp.259-276.
- [13] Zhou, D.; Blunt, M. y Orr, F. Jr. Hydrocarbon Drainage along Corners of Noncircular Capillaries. *J. of Colloid and Interface Science*, Vol. 187, 1997, pp.11-21.
- [14] Illingworth, T.C.; Golosnoy, I.O. Numerical solutions of diffusion-controlled moving boundary problems which conserve solute. *Journal of Computational Physics*, Vol. 209, N1, 2005, pp. 207-225.
- [15] Hines, A.; Maddox, R. *Transferencia de Masa: Fundamentos y Aplicaciones*. Prentice Hall, 1987.
- [16] Bejan, A. *Heat Transfer*. John Wiley & Sons, 1995.
- [17] Unlusu, Betul; Sunol, Aydin K. Modeling of equilibration times at high pressure for multicomponent vapor-liquid diffusional processes. *Fluid Phase Equilibria*. Vol. 226, 2004, pp. 15-25.
- [18] Sassi, M.; Raynaud, M. Solution of the moving-boundaries problems. *Numerical Heat Transfer Part B*, Vol.34, 1998, pp.271-286.
- [19] Wilke, C.; Lee. *Ind.Eng.Chem.* Vol.47, 1955, pp.1253.

- [20] Pitzer, K.S.; Sterner, S.M. Equations of state valid continuously from zero to extreme pressures for H<sub>2</sub>O and CO<sub>2</sub>. *J.Chem.Phys.* Vol. 101 (4), 1994, pp. 3111-3116.
- [21] Reamer, H.; Sage, B. Phase equilibria in hydrocarbon systems. Volumetric and phase behavior of the n-decane-CO<sub>2</sub> system. *J.Chem.Eng.Data.* Vol. 8, 1963, pp. 508-513.
- [22] Zabala, D.; López de Ramos, A. Gas-Liquid Interface Displacement: Numerical and experimental comparative analysis for carbon dioxide diffusion into n-decane. Paper 538-229, presented at *4th IASME / WSEAS Int. Conf. on FLUID MECHANICS and AERODYNAMICS*, Crete, Greece, Aug. 21-23, 2006.
- [23] Scheibel, E.G. *Ind.Eng.Chem.* Vol.46, 1954, pp. 2007.